URSI-B EMTS 2025, Bologna, 23–27 June

High-Gain mm-Wave Leaky-Wave/Fabry-Perot Antenna Using Substrate-Integrated Partially Reflective Surfaces

Rana Muhammad Hasan Bilal(1), Stefano Moscato(2), Simone Genovesi(1), Giuliano Manara(1), and Filippo Costa(1)
(1) Department of Information Engineering, University of Pisa, 56125 Pisa, Italy.
(2) Research and Development Department of SIAE MICROELETTRONICA, Via Michelangelo Buonarroti, 21, Cologno Monzese (MI), Italy.

Abstract

Leaky-wave/Fabry-Perot antennas (LWAs/FPAs) are often implemented by using an air-spacer cavity between the ground plane and partially reflective surfaces (PRSs), which complicates the fabrication process. In this paper, a substrate integrated FPA is investigated by employing a design topology comprising a top PRS printed onto a metal backed low-cost ITERA MT40 dielectric substrate. The top PRS consists of a periodic array of simple patches that are etched by using the standard photolithography method. A pair of metallic strips are introduced in the slotted ground-plane to achieve good impedance matching. The proposed FPA achieves a high gain of 11 dBi and shows a simulated impedance matching with an $|S_{11}|$ value of -18 dB at 85 GHz. Finally, the antenna is fabricated and its simulation results are validated through multiple measurements conducted on various samples.

1 Introduction

FP antennas are extensively studied for high-gain applications, including satellite communication [1], remote sensing [2], radar detection [2], and astronomy [3]. They have proven to be an effective solution for such applications because of their simple and easily fabricable design, which incorporates an air cavity positioned at half the wavelength between the ground plane and the top PRS [4, 5]. The most significant and straightforward aspect of these antennas is their excitation, as they can be easily fed using a simple waveguide source, eliminating the need for a complex feeding network typically required in multiple-input multiple-output (MIMO) antenna arrays. In the past, various design approaches for implementing FP antennas have been studied and include dielectric superstrates [6, 7], electromagnetic band-gap structures [8, 9], multiple-layer PRS [10, 11] and single-layer PRS [12, 13] etc.

Among the various design methods for FP antennas, the PRS-based approach stands out as the most practical and straightforward. This is due to its simple geometry, easy fabrication process, and simple feeding mechanism [14]. The simplest and most standard design topology for PRS-based FP antennas consists of metallic patches [15] and slots [16], due to their ease of design and fabrication. Although FPAs are highly suitable for high-gain applications, they typically require an air spacer between the ground plane and the top PRS [17–19]. This configuration poses significant fabrication challenges such as precise alignment and careful mechanical design and is difficult to handle. Numerous FPAs have been studied and explored, incorporating air cavities in their design configurations, as reported in [10, 11, 20–23]. However, these designs cannot be integrated with planar systems or printed circuit boards (PCBs).

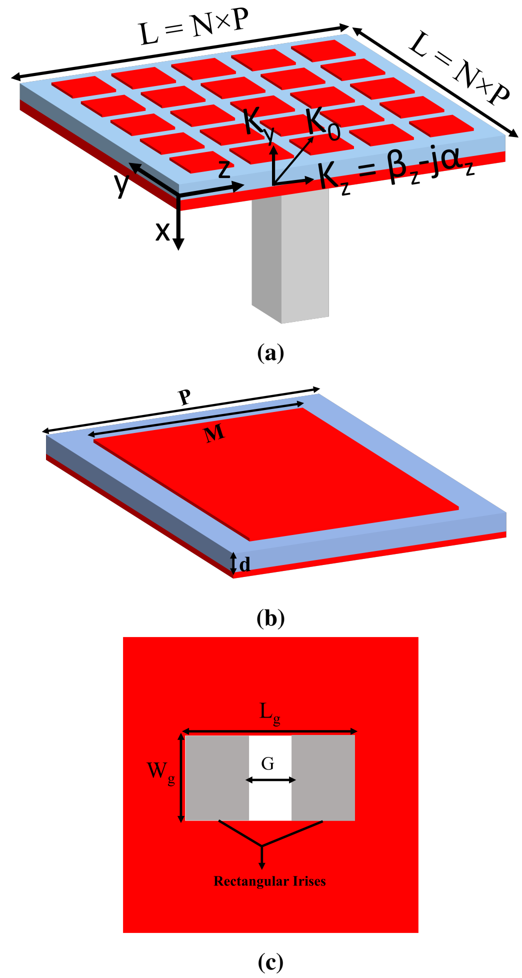

Figure 1. 3D illustration of the FPA with a total size (L×L) of 31 mm × 31 mm with N shows the number of PRS elements and P denotes the periodicity of the unit cell, (b) Side view of the unit cell with, P = 1 mm, M = 0.875 mm and d = 1 mm, (c) Back view of the FPA, indicating the pair of metallic matching strips with L_g = 3.098 mm, W_g = 1.54 mm and G = 0.90 mm.

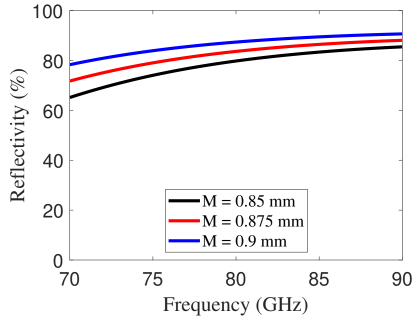

Figure 2. Reflectivity of the proposed unit cell described in Fig. 1b over varying size of the top patch.

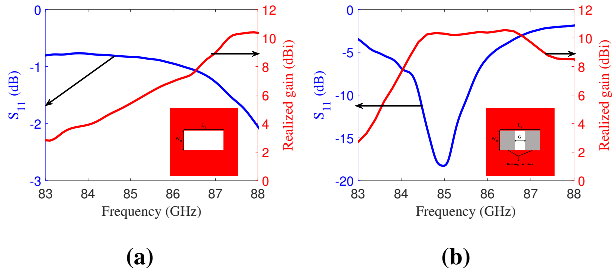

Figure 3. (a) $|S_{11}|$ and realized gain with open waveguide and (b) $|S_{11}|$ and realized gain with a pair of metallic strips. Inset shows the back view of the proposed FPA.

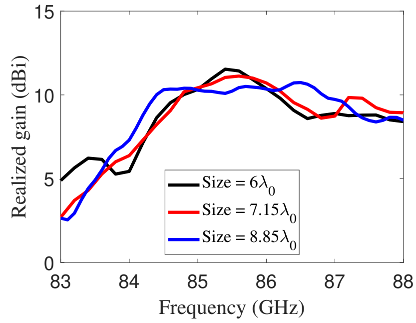

Figure 4. Realized gain of the proposed FPA over varying sizes.

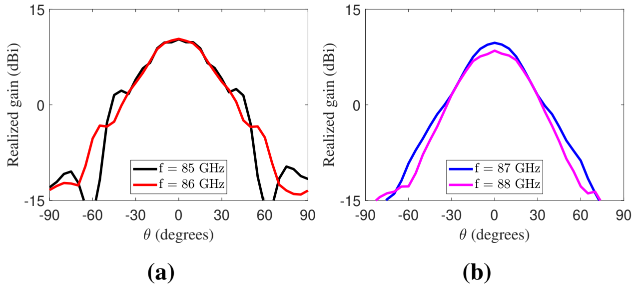

Figure 5. Radiation patterns of the proposed FPA at different operating frequencies: (a) f_0 = 85 and 86 GHz, (b) f_0 = 87 and 88 GHz.

Most of the existing FPAs are designed for the microwave frequency spectrum, extending up to the Ka band. However, there is growing interest in the millimeter-wave (mm-wave) frequency range due to its numerous use cases and applications, which require moderate gain, low-profile, and high customizable antenna arrays. FPAs are promising candidates to meet these requirements. It is essential to design FPAs specifically tailored for the mm-wave spectrum, with particular emphasis on the E-band, as it serves as the current standard for multi-Gigabit connections in point-to-point links and is foreseen to be exploited in 6G radio access. To integrate smoothly with PCBs and planar systems, these antennas should be fabricated on a substrate, unlike traditional FPAs that rely on air-spacer cavities.

In this paper, the authors aim to design and fabricate an FPA on a dielectric substrate made of ITERA MT40, positioned between the ground plane and the top PRS. The top PRS consists of an array of metallic patches, making its design configuration straightforward and easy to fabricate. Additionally, a notable feature of this FPA is its simple waveguide feeding mechanism, in contrast to previous FPAs that relied on aperture-coupled or coplanar slot feeding techniques.

2 Antenna Layout

The schematic representation of the proposed FPA is shown in Fig. 1. It includes the complete antenna structure (Fig. 1a), a side view of the PRS unit cell (Fig. 1b), and a back view of the antenna (Fig. 1c). The FPA comprises a top PRS, consisting of a periodic array of the capacitive patches which are printed onto a dielectric substrate of ITERA MT40 from Isola group ($\varepsilon_r = 3.45$, $\tan\delta = 0.0027$). The dielectric substrate is covered with a the slotted ground plane and a pair of metallic strips used for impedance matching. The copper thickness is used here is 0.35 mm. The design and numerical simulation of the FPA is performed by using the time-domain solver of the CST studio software from Dassault system.

3 Results and Discussion

The basic principle behind these types of FPA is the selection of PRS with reflectivity around 90%, which allows us to establish the resonant cavity between the bottom ground plane and the top PRS. The top PRS optimizes its reflectivity to focus energy toward the main lobe. Without PRS, energy radiates isotropically, leading to increased side lobes. To achieve high antenna directivity, the PRS unit cell is optimized for partial reflection characteristics, as illustrated in Fig. 1b. The reflectivity of the patch-based unit cell is analyzed by varying the size of the patch, as depicted in Fig. 2.

Once the desired reflectivity of the PRS unit cell is achieved, the next step is to design the antenna, which consists of an array of 31×31 square patches with an overall size of 31 mm $\times$ 31 mm. The performance metrics of the designed antenna, including $|S_{11}|$ and realized gain, are simulated and presented in Fig. 3. For comparison, Fig. 3a shows the $|S_{11}|$ and realized gain of the antenna without the inclusion of the metallic strips. It is observed that the antenna exhibits poor impedance matching, with an $|S_{11}|$ value of -1 and a realized gain of 10 dBi at higher operating

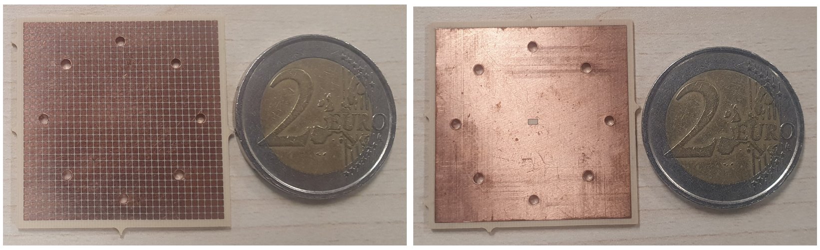

(a) (b)

Figure 6. Fabricated sample of the proposed FPA with a size of 31 mm × 31 mm: (a) Front view of the FPA showing an arrays of square patches-based PRS and (b) Back view of the FPA, showing waveguide alignment holes and the slot in the ground-plane.

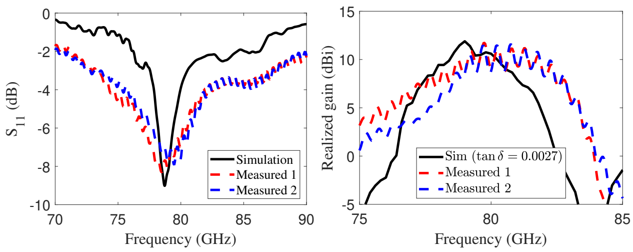

(a) (b)

Figure 7. Comparison of the full-wave Simulation and measured (a) $|S_{11}|$ (b) realized gain of the FPA. Measurements are conducted on two different prototypes to verify the replicability of results and fabrication tolerances.

frequencies. To achieve the desired impedance matching, a pair of metallic strips are incorporated into the bottom ground plane, as illustrated in the inset of Fig. 3b. Fig. 3b shows that the antenna achieves impedance matching, with an $|S_{11}|$ value of -19 dB and a realized gain of 11 dBi at 85 GHz.

The gain is analyzed for various antenna sizes, as shown in Fig. 4. The proposed FPA demonstrates a broader bandwidth for $8.85\lambda_0$ compared to other sizes. While the other antenna sizes also exhibit reasonable bandwidths, the larger size is selected to accommodate alignment holes in the ground plane for waveguide assembly. Furthermore, the antenna radiation patterns at different operating frequencies—85 GHz, 86 GHz, 87 GHz, and 88 GHz—are simulated and presented in Fig. 5. The results demonstrate that the antenna maintains a stable radiation pattern with high directivity, particularly in the boresight direction.

4 Fabrication and Measurements

In this section, the performance of the antenna is validated by fabricating an array of 31 × 31 square patches with an overall size of 31 mm × 31 mm. The patches are fabricated on a low-loss dielectric substrate of ITERA MT40 using the standard photolithography fabrication method. During fabrication, alignment holes are created to accommodate the rectangular waveguide, considering the size of the flange for proper excitation, as illustrated in the fabricated prototypes shown in Fig. 6b.

To verify the simulation results of the proposed antenna, measurements were performed on multiple samples of the same antenna to ensure a fair evaluation. The fabricated antenna sample is illustrated in Fig. 6, divided into two sections: Fig. 6a presents the front view of the antenna, Fig. 6b shows the back view featuring alignment holes for positioning the rectangular waveguide.

During the measurement of multiple samples, a discrepancy was observed in the dielectric constant of the ITERA MT40 substrate. This discrepancy was identified because the measured $|S_{11}|$ values deviated from the simulated results. To verify this, multiple samples were fabricated and their characteristics are measured, revealing that the fabricated antenna exhibited peak performance at 79 GHz instead of the expected 85 GHz. Consequently, the dielectric constant of the simulated substrate was adjusted in the simulation to achieve resonance at 79 GHz, leading to an estimated dielectric constant of approximately 4.3. The modified simulation results were compared with the measured results, including $|S_{11}|$ and realized gain. As shown in Fig. 7a, the simulated and measured $|S_{11}|$ values closely align. Similarly, the gain comparison, presented in Fig. 7b, also demonstrates a close match between the two.

5 Conclusion

This paper reported a simple, low profile, substrate-integrated FPA fabricated on a low-loss ITERA MT40 dielectric substrate using standard photolithography. Unlike previously reported FP antennas, this design featured an air-cavity-free structure, which reduced design complexity and enhanced compatibility with PCB and microstrip circuits. It operated in the E-band of the mm-wave frequency range, achieved a high gain of 11 dBi, and demonstrated excellent impedance matching with an $|S_{11}|$ level of -18 dB. Performance metrics, such as $|S_{11}|$ and realized gain of the FPA were validated through experimental measurements.

References

[1] E. Arnieri, L. Boccia, G. Amendola, and G. Di Massa, "A compact high gain antenna for small satellite applications," *IEEE Transactions on Antennas and Propagation*, vol. 55, no. 2, pp. 277–282, 2007.

[2] F. Qin, S. S. Gao, Q. Luo, C.-X. Mao, C. Gu, G. Wei, J. Xu, J. Li, C. Wu, K. Zheng *et al.*, "A simple low-

cost shared-aperture dual-band dual-polarized high-gain antenna for synthetic aperture radars," *IEEE Transactions on Antennas and Propagation*, vol. 64, no. 7, pp. 2914–2922, 2016.

[3] H. W. Ehrenspeck, *High-Gain UHF Backfire Antenna for Communications, Telemetry, and Radio Astronomy*. Air Force Cambridge Research Laboratories, Office of Aerospace Research . . . , 1967, no. 129.

[4] M. Garcia-Vigueras, J. L. Gomez-Tornero, G. Goussetis, A. R. Weily, and Y. J. Guo, "1D-leaky wave antenna employing parallel-plate waveguide loaded with PRS and HIS," *IEEE Transactions on Antennas and Propagation*, vol. 59, no. 10, pp. 3687–3694, 2011.

[5] A. T. Almutawa, A. Hosseini, D. R. Jackson, and F. Capolino, "Leaky-wave analysis of wideband planar Fabry-Perot cavity antennas formed by a thick PRS," *IEEE Transactions on Antennas and Propagation*, vol. 67, no. 8, pp. 5163–5175, 2019.

[6] N. Wang, L. Talbi, Q. Zeng, and J. Xu, "Wideband Fabry-Perot resonator antenna with electrically thin dielectric superstrates," *IEEE Access*, vol. 6, pp. 14 966–14 973, 2018.

[7] T. Kaji, H. Sato, Q. Chen, S. Nagae, A. Kumagai, and O. Kagaya, "A leaky wave antenna with dielectric superstrate on perforated dielectric spacer," *IEEE Transactions on Antennas and Propagation*, vol. 71, no. 6, pp. 4843–4850, 2023.

[8] Z.-C. Ge, W.-X. Zhang, Z.-G. Liu, and Y.-Y. Gu, "Broadband and high-gain printed antennas constructed from Fabry-Perot resonator structure using EBG or FSS cover," *Microwave and Optical Technology Letters*, vol. 48, no. 7, pp. 1272–1274, 2006.

[9] T.-H. Vu, S. Collardey, A.-C. Tarot, and K. Mahdjoubi, "Input impedance of Fabry-Perot, EBG, and leaky-wave antennas excited by a line source," *IEEE Antennas and Wireless Propagation Letters*, vol. 8, pp. 248–252, 2009.

[10] N. Wang, Q. Liu, C. Wu, L. Talbi, Q. Zeng, and J. Xu, "Wideband Fabry-Perot resonator antenna with two complementary FSS layers," *IEEE Transactions on Antennas and Propagation*, vol. 62, no. 5, pp. 2463–2471, 2014.

[11] M. W. Niaz, Y. Yin, R. A. Bhatti, Y.-M. Cai, and J. Chen, "Wideband Fabry-Perot resonator antenna employing multilayer partially reflective surface," *IEEE Transactions on Antennas and Propagation*, vol. 69, no. 4, pp. 2404–2409, 2020.

[12] A. Hosseini, F. De Flaviis, and F. Capolino, "A 60 GHz simple-to-fabricate single-layer planar Fabry-Perot cavity antenna," *IET Microwaves, Antennas & Propagation*, vol. 9, no. 4, pp. 313–318, 2015.

[13] R. M. H. Bilal, M. Borgese, S. Genovesi, G. Manara, and F. Costa, "High directional Fabry-Perot millimeter-wave antenna for D-band spectrum," pp. 1–4, 2024.

[14] F. Costa, D. Bianchi, A. Monorchio, and G. Manara, "Linear Fabry-Perot/leaky-wave antennas excited by multiple sources," *IEEE Transactions on Antennas and Propagation*, vol. 66, no. 10, pp. 5150–5159, 2018.

[15] T. Zhao, D. R. Jackson, J. T. Williams, H.-Y. Yang, and A. A. Oliner, "2D periodic leaky-wave antennas-Part I: metal patch design," *IEEE Transactions on Antennas and Propagation*, vol. 53, no. 11, pp. 3505–3514, 2005.

[16] T. Zhao, D. R. Jackson, and J. T. Williams, "2D periodic leaky-wave antennas-Part II: Slot design," *IEEE Transactions on Antennas and Propagation*, vol. 53, no. 11, pp. 3515–3524, 2005.

[17] R. Sauleau, P. Coquet, T. Matsui, and J.-P. Daniel, "A new concept of focusing antennas using plane-parallel Fabry-Perot cavities with nonuniform mirrors," *IEEE Transactions on Antennas and Propagation*, vol. 51, no. 11, pp. 3171–3175, 2003.

[18] Y. Coulibaly, M. Nedil, L. Talbi, and T. A. Denidni, "Design of high gain and broadband antennas at 60 GHz for underground communications systems," *International Journal of Antennas and Propagation*, vol. 2012, no. 1, p. 386846, 2012.

[19] L.-Y. Ji, P.-Y. Qin, and Y. J. Guo, "Wideband Fabry-Perot cavity antenna with a shaped ground plane," *IEEE Access*, vol. 6, pp. 2291–2297, 2017.

[20] H. Vettikalladi, O. Lafond, and M. Himdi, "High-efficient and high-gain superstrate antenna for 60 GHz indoor communication," *IEEE Antennas and Wireless Propagation Letters*, vol. 8, pp. 1422–1425, 2009.

[21] K. Konstantinidis, A. P. Feresidis, P. S. Hall, and M. J. Lancaster, "Design of Fabry-Perot cavity antenna at 94 GHz," in *2012 Loughborough Antennas & Propagation Conference (LAPC)*. IEEE, 2012, pp. 1–4.

[22] A. Hosseini, F. Capolino, and F. De Flaviis, "Gain enhancement of a V-band antenna using a Fabry-Perot cavity with a self-sustained all-metal cap with FSS," *IEEE Transactions on Antennas and Propagation*, vol. 63, no. 3, pp. 909–921, 2014.

[23] H. Attia, M. L. Abdelghani, and T. A. Denidni, "Wideband and high-gain millimeter-wave antenna based on FSS Fabry-Perot cavity," *IEEE Transactions on Antennas and Propagation*, vol. 65, no. 10, pp. 5589–5594, 2017.